JOURNAL OF GEOPHYSICAL RESEARCH, VOL. 99, NO. D6, PAGES 12,963–12,980, JUNE 20, 1994

Influence of the vertical structure of the atmosphere on the seasonal variation of precipitable water and greenhouse effect

Sandrine Bony

Laboratoire de Météorologie Dynamique du Centre National de la Recherche Scientifique, Paris

Jean-Philippe Duvel

Laboratoire de Météorologie Dynamique du Centre National de la Recherche Scientifique
Palaiseau, France

Abstract. By using satellite observations and European Centre for Medium Range Weather Forecasts analyses, we study the seasonal variations of the precipitable water and the greenhouse effect, defined as the normalized difference between the longwave flux emitted at the surface and that emergent at the top of the atmosphere. Results show a strong systematic influence of the vertical structure of the atmosphere on geographical and seasonal variations of both precipitable water and greenhouse effect. Over ocean, in middle and high latitudes, the seasonal variation of the mean temperature lapse rate in the troposphere leads to large seasonal phase lags between greenhouse effect and precipitable water. By contrast, the seasonal variation of the clear-sky greenhouse effect over tropical oceans is mainly driven by the total atmospheric transmittance and thus by precipitable water variations. Over land, the seasonal variation of the tropospheric lapse rate acts to amplify the radiative impact of water vapor changes, giving a strong seasonal variation of the greenhouse effect. Over tropical land regions, monsoon activity generates a seasonal phase lag between surface temperature and relative humidity variations that gives a seasonal lag of about 2 months between the surface temperature and the clear-sky greenhouse effect. Generally, the cloudiness amplifies clear-sky tendencies. Finally, as an illustration, obtained results are used to evaluate the general circulation model of the Laboratoire de Météorologie Dynamique.

1. Introduction

The complex behavior of the various feedbacks involved when an external or internal forcing is applied to the climate system has been investigated by using either general circulation models (GCM) [e.g., *Hansen et al.*, 1984; *Wetherald and Manabe*, 1988] or one-dimensional radiative-convective models. A recent GCM intercomparison [*Cess et al.*, 1990] shows agreement among different GCM estimates of sensitivity of the clear-sky Earth radiation budget to a global surface temperature change. If we consider that this clear-sky sensitivity is mainly related to change in the outgoing longwave flux, this result tends to demonstrate that different GCMs (and thus various sets of parameterizations) give a similar global greenhouse effect response to a surface temperature change. Globally, the greenhouse effect is not only a tracer of the atmospheric opacity but also of the vertical structure of the atmosphere that depends mainly on convective and radiative processes together with the mean sensible and latent heat fluxes at the surface. Although compensating effects may appear, especially for changes in the vertical distribution of both water vapor and temperature, the different GCMs studied by *Cess et al.* [1990] thus seem to respond similarly to a surface temperature change.

The problem is that there is no observation available to validate the complex interactions involved in GCM sensitivity tests (for example, by increasing trace gas concentration or by changing the global surface temperature). The relations between the surface temperature, the precipitable water and the clear-sky greenhouse effect that can be extracted from available satellite observations are averages over an ensemble of local-regional relations and have no obvious reason to be adapted for the evaluation of a modeled global climate change. This is mainly because these local relations do not correspond to an equilibrium state between the atmospheric column and fluxes at the surface and at the top of the column. The local atmospheric structure is actually strongly influenced by the general (mainly meridional) circulation. Also, the local sea surface temperature (SST) is strongly influenced by the ocean circulation and is not only related to the local net flux at the sur-

Paper number 94JD00482.
0148-0227/94/94JD-00482$05.00

face. In the context of global change only, the results of recent observational studies [*Raval and Ramanathan,* 1989; *Stephens and Greenwald,* 1991; *Duvel and Bréon,* 1991] are thus not directly usable to validate the magnitude of GCM water vapor feedbacks. This is confirmed by the different magnitudes of the relation between the SST and the greenhouse effect obtained from interannual [*Duvel and Bréon,* 1991] or geographical [*Raval and Ramanathan,* 1989] variabilities, especially over middle and high latitudes.

By using time series of observed outgoing clear-sky longwave flux, it is nevertheless possible to study the influence of the variability of the atmospheric structure on the greenhouse effect at different time scales (i.e., seasonal, interannual,...). This is expected to furnish useful information on the different processes involved in greenhouse effect sensitivity. For example, it is interesting to uncover coherent behavior explaining part of the relatively strong scatter found in previous observations of the local relation between the surface temperature, the precipitable water and the greenhouse effect. From these coherent behaviors, one may extract useful information on systematic aspects of the variability of the atmospheric structure in different weather regimes (i.e., tropics, mid-latitudes, subtropical subsidence zones,...). In addition, and it is the principal aim of the Atmospheric Model Intercomparison Program [*Gates,* 1992], we can use observable variabilities (i.e., geographical, seasonal, interannual) to evaluate GCM simulations made with the same boundary conditions, i.e., SST and insolation. The seasonal variation of the greenhouse effect is driven by the seasonal variation of the numerous processes (convection, vertical diffusion, radiation, ...) that modify the temperature and water vapor profiles. Validation of this seasonal variation is thus an evaluation of the GCM representation of many processes and may be used as a basis to improve the physical parameterizations.

A description of the data set used is described in section 2. In section 3 we study the observed seasonal variations of precipitable water and greenhouse effect over ocean. We show how the precipitable water and the clear-sky greenhouse effect are related to changes in the surface temperature and in the vertical structure of the atmosphere, i.e., temperature and relative humidity profiles. A similar analysis is also performed over land regions (section 4). The impact of the cloudiness on the results is briefly discussed in section 5. In section 6 we show how the observed results can be used to evaluate the seasonal variation simulated by a general circulation model. Summary and discussion are reported in section 7.

2. Satellite Observations, European Centre for Medium Range Weather Forecasts Analyses and Analysis Method

Satellite Observation

Observations of clear-sky and total outgoing longwave (LW: 5 to 50 μm) fluxes are derived from the Earth Radiation Budget Experiment (ERBE) [*Barkstrom,* 1984]. We use information received by the scanners on board the operational Sun-synchronous satellite NOAA 10 and the Earth Radiation Budget Satellite ERBS (in a 57° inclination orbit) for each 2.5°x2.5° region during the year 1988. These are monthly means, archived in validated "S4" products [*Barkstrom et al.,* 1989]. The detection of clear-sky scenes, based on the ERBE scene identification procedure, is difficult in regions characterized by nearly permanent cloud conditions (such as over the Intertropical Convergence Zone (ITCZ)) or by the presence of snow or ice because of the low contrast between snow and cloud albedo. *Harrison et al.* [1990] discuss the accuracy of ERBE measurements and suspect regional monthly means of LW fluxes to have an rms error of 2 W/m^2 in clear-sky conditions, and 3 W/m^2 otherwise. Systematic bias errors for total LW fluxes are estimated to be less than 1 W/m^2, whereas clear-sky LW fluxes are suspected to be overestimated by about 4 W/m^2.

Columnar water vapor data used in this study are derived from the SSM/I (Special Sensor Microwave Imager) instrument, following the algorithm developed by *Wentz* [1983]. As with many other microwave measurements, data are useful only over open oceans. *Esbensen et al.* [1993] reviewed in detail what is known about the accuracy of these data. Based on comparisons with in situ radiosonde measurements, Wentz retrievals of precipitable water are estimated to have an rms error of 3 kg/m^2. Since only three spectral channels are available on SSM/I, columnar water vapor retrievals can not be based on actual vertical profiles of humidity and temperature, and thus empirical atmospheric profiles are used. Systematic error of the *Wentz* [1983] physically based retrieval associated with simplifications in the assumed vertical structure of the atmosphere has been estimated by *Sun* [1993] and found to be an overestimate of about 3 kg/m^2 over large-scale areas in all latitudes.

Monthly means of sea surface temperature used in this study are blended in situ (ship and buoy) and satellite data analyzed by *Reynolds* [1988]. The average rms monthly error is estimated to be 0.78°C, and the average of the absolute value of the monthly bias is 0.09°C. Over land, we use land surface temperature data derived from the International Satellite Cloud Climatology Project (ISCCP) monthly mean products (so-called C2 products, see *Rossow and Schiffer* [1991] for a precise description). Comparison with weather stations data leads one to suspect satellite-derived temperatures to be overestimated by around 0.9°C [*Rossow and Garder,* 1993].

ECMWF Analyses

We use monthly mean values of surface pressure, surface temperature and of temperature and specific humidity at eight standard pressure levels (i.e., 1000, 850, 700, 500, 400, 300, 200, 100 mbar) derived from the European Centre for Medium Range Weather Forecasts (ECMWF) for the year 1988. The temperature, specific humidity and the pressure of the lowest boundary of the first layer is set to surface values. During the year 1988,

no major modification was made to the ECMWF model [*Arpe*, 1990], so that these analyses can be used to study the seasonal variation.

Analysis Method

In this paper only monthly means of all observed or simulated quantities are considered.

The greenhouse effect. The normalized greenhouse effect parameter used in this study is that defined by *Raval and Ramanathan* [1989] as

$$g_c = \frac{\sigma T_s^4 - \mathrm{LW}_c}{\sigma T_s^4} \tag{1}$$

where T_s is the surface temperature, σ the Stefan's constant and LW_c the clear-sky outgoing longwave flux ($\mathrm{W/m^2}$). The total greenhouse effect is obtained by replacing LW_c by the mean longwave flux (i.e,, clear plus cloudy). The outgoing longwave flux may be separated into two parts representing the direct contribution of the surface flux (i.e., $\tau_s \sigma T_s^4$ where τ_s is the total atmospheric transmittance between the surface and the top of the atmosphere) and the LW atmospheric emission to space (E_a). The normalized greenhouse effect may thus be expressed as

$$g = (1 - \tau_s) - \frac{\mathrm{E}_a}{\sigma T_s^4} = g_s - e_a \tag{2}$$

where g_s corresponds to the greenhouse effect resulting from the total atmospheric transmittance and e_a to the normalized atmospheric longwave emission that reduces the value of g.

Water vapor fluctuations. The water vapor content of the atmosphere is determined both by the saturation water vapor pressure (q_o) and the relative humidity (r). The seasonal variation of temperature profiles is a fundamental driving factor for the seasonal variation of humidity profiles. For each month and each pressure level p, we can define two different values for the monthly mean specific humidity $q(p)$ corresponding to monthly change due only to seasonal variation of temperature or relative humidity, i.e., respectively,

$$q^T(p) = \overline{r}(p)\, q_o(T(p)) \tag{3}$$

$$q^r(p) = r(p)\, q_o(\overline{T}(p)) \tag{4}$$

where the overbar stands for annual averages. In order to examine the origin of the impact of temperature variations on $q(p)$, the monthly mean temperature at each vertical level can also be separated into

$$T^\Gamma(p) = T(p) - \Delta T_s \tag{5}$$

$$T^s(p) = \overline{T}(p) + \Delta T_s \tag{6}$$

where ΔT_s is the monthly deviation of the surface temperature. By defining Δ as the monthly deviation from annual mean, we obtain $\Delta T^s(p) = \Delta T_s$ and $\Delta T^\Gamma(p) = \Delta T(p) - \Delta T_s$. Thus ΔT^Γ accounts for changes in the shape of the temperature profile (noted Γ in reference to the lapse rate Γ=-dT/dz but including all shape changes) and ΔT_s accounts for vertically uniform temperature changes. The term q^T can thus be divided into

$$q^{T_s}(p) = \overline{r}(p)\, q_o(T^s(p)) \tag{7}$$

$$q^\Gamma(p) = \overline{r}(p)\, q_o(T^\Gamma(p)) \tag{8}$$

At first order, the monthly deviations of each of the terms (q^r, q^{T_s}, q^Γ) are additive. By integrating these terms over the whole atmospheric column, the monthly deviation of the precipitable water W is well approximated by

$$\Delta W = \Delta^{T_s} W + \Delta^\Gamma W + \Delta^r W \tag{9}$$

The mass-weighted lapse rate. Although the temperature lapse rate may vary with altitude, it is convenient to characterize the rough shape of the temperature profile by considering a mean mass-weighted lapse rate in the troposphere Γ_m [*Stone and Carlson*, 1979; *Yang and Smith*, 1985] defined as

$$\Gamma_m = \frac{1}{M} \int_0^{z(200\ mbar)} \frac{dT}{dz}\, \rho(z) dz \tag{10}$$

where M is the mass of the air column (of surface unity) from the surface to 200-mbar level, and $r(z)$ the air density at the altitude z.

The Fourier analysis. Although the seasonal cycle of a climatic variable may have a variety of shapes, it is often convenient to consider only the first harmonic (i.e., 12 month period) of the seasonal variation because it can be described only by its amplitude and its phase. This is justified whenever most of the seasonal variance is explained by the first harmonic. For the different quantities considered in this study (i.e., SST, W, g) and for most latitudes, the zonal mean seasonal cycle may be well represented by its first harmonic (not shown) with variance percentages larger than 90%. Low percentages of variance are only obtained over equatorial regions or for highest latitudes, with nevertheless values larger than 50%. In this paper this analysis method is used to highlight the main seasonal characteristics (amplitude and phase) of zonal mean quantities. The seasonal amplitude is defined has $A_s = \sqrt{2H_{1s}}$ where H_{1s} is the variance of the first harmonic.

All along the analysis, a region for a given month is considered only if all observed quantities (i.e., SST, LW_c, LW, W) are defined for this month and if there is no ice over ocean. A latitude band is considered in the spectral analysis if at least half of the nominal number of regions for this latitude are defined for each of the 12 months.

3. The Observed Seasonal Cycle Over Ocean

Seasonal Variations of the Precipitable Water

The hypothesis of a link between the sea surface temperature (SST) and the precipitable water (W) is based primarily on the variation of the saturation water vapor

pressure at the surface (q_{s_o}) with the surface temperature through the Clausius-Clapeyron relation. This relation modifies the water vapor storage capacity of the lowest layers of the atmosphere. However, there is no reason for humidity profiles, together with the depth of the boundary layer, to be rigorously related to the local SST, so that precipitable water may vary even for a fixed SST [*Prabhakara et al.*, 1979; *Liu*, 1986; *Stephens*, 1990]. This variation is inspected here for different SST intervals and for both SSM/I data and ECMWF analyses (Figure 1a). Because of the exponential variation of saturation water vapor at the surface (q_{s_o}) as a function of SST, we use fixed q_{s_o} intervals rather than fixed SST intervals. This makes it possible to compare the standard deviation of the precipitable water from one SST interval to another. Figure 1a exhibits clearly the well-known increase of the precipitable water with the SST. The spread of the SSM/I precipitable water distribution appears to be much larger for warm regions than for cold ones. For a same q_{s_o} interval of 2 g/kg, the standard deviation of W is twice as large (about 7.5 kg/m^2) for SST of 25°C than for SST around 15°C. This result is in agreement with observations of *Gaffen et al.* [1992a] showing, on the basis of radiosonde data, that the relation between the SST and W is better defined for cold than for warm regions.

The breadth of the precipitable water distribution (and also the mean W-SST slope) is likely to be explained by seasonal and regional changes in the planetary boundary layer (PBL) depth, and more generally by changes in temperature and water vapor profiles, rather than by changes in moisture divergence, even if the atmospheric structure is somewhat related to it. This is because at the monthly scale, water vapor divergence or convergence is nearly balanced by rain and local evaporation. The large scatter of W in tropical regions may tentatively be explained by the large variability of both PBL depth and relative humidity profiles because convective as well as subsidence regions can coexist within a single SST interval. Over middle and high latitudes, maybe because there is a more zonal distribution of both SST and weather types, the precipitable

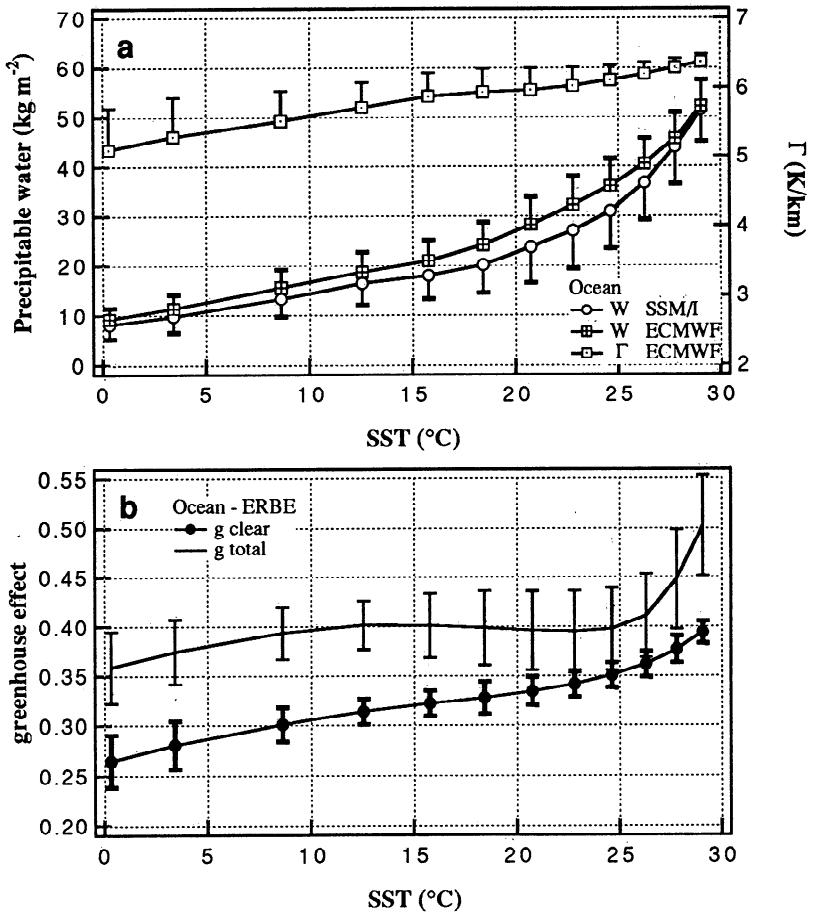

Figure 1. (a) Mean precipitable water (derived from SSM/I data and produced by ECMWF analyses) averaged for the year 1988 in different sea surface temperature (SST) intervals, corresponding to regular intervals of surface saturation humidity. Also reported is the mean mass-weighted tropospheric lapse rate (in Kelvin per kilometer) derived from ECMWF analyses over ocean for the same period. Vertical bars indicate the half standard deviation within each saturation specific humidity interval. (b) Same as Figure 1a but for the clear-sky and total normalized greenhouse effect derived from ERBE data for the year 1988.

water is better related to the SST. One may thus expect a better seasonal relation between the SST and W in middle and high latitudes than in tropical regions.

Seasonal phases and amplitudes of the zonal mean precipitable water estimated by SSM/I are reported on Figures 2a and 2b, respectively. The SST has a strong impact on the seasonal phase of W since, for all considered latitudes, there is a phase lag smaller than 1 month between W and the SST. Seasonal amplitudes of both W and SST are maximal in the northern hemisphere (NH) with maximum values at 40°N. However, there is no obvious agreement between the seasonal amplitudes of W and SST, especially when comparing tropics to mid-latitudes. This suggests that the seasonal amplitude of the precipitable water is not only related to the seasonal amplitude of the SST but also to the seasonal variation of the atmospheric vertical structure.

In agreement with *Liu et al.* [1991], the precipitable water estimated by ECMWF analyses (Figure 1a) is overestimated with regard to SSM/I estimates, especially over subtropical ocean (i.e., SST between 20° and 25°C). By contrast, the standard deviation of W is smaller for ECMWF analyses. However, by comparing Figures 2 and 3, there is a good agreement between SSM/I and ECMWF for both seasonal phase and amplitude of the zonal W averages. This makes it possible to analyze with good confidence the origin of the seasonal cycle of the precipitable water by using ECMWF analyses. This origin is analyzed using the method described in section 2 (equations (3)-(9)). In middle latitudes, the influence of the vertically uniform temperature changes is predominant, especially for the southern hemisphere (SH) where both amplitude and phase of $\Delta^{T_s}W$ are very close to the actual amplitude and phase of ΔW (Figure 3).

Between 5° and 15°N, the seasonal cycle of the relative humidity profiles is the principal source for the seasonal variation of the precipitable water. More generally, in accordance with observations of *Gaffen et al.* [1992b] based on radiosonde data, the seasonal variation of W in the tropics is strongly influenced by relative humidity variations. On the opposite, the seasonal variation of the precipitable water in middle and high latitudes is poorly influenced by the relative humidity and the large phase difference between $\Delta^r W$ and $\Delta^{T_s}W$ has thus a very weak impact on both seasonal phase and amplitude of the precipitable water. In the tropics, the mean relative humidity is in phase with the surface temperature and thus enhances the seasonal amplitude of the precipitable water. Note that this result is a tendency obtained over global ocean by using zonal means. However, when considering individual regions over the ITCZ there is a poor relationship between the surface temperature and the precipitable water that depicts a nonsystematic influence of the surface temperature on the convective or subsiding nature of the region, even for monthly means. Note that, taking SSM/I estimates as a reference, the underestimate of the seasonal amplitude of the ECMWF precipitable water in the tropics (i.e., comparing Figures 2b and 3b) may be mostly attributed to a too weak impact of relative humidity variations.

The seasonal amplitude of $\Delta^\Gamma W$ increases poleward (Figure 3b), leading to an equal contribution of $\Delta^{T_s}W$ and $\Delta^\Gamma W$ around 50°. It is worth noting that the lapse rate and $\Delta^\Gamma W$ vary nearly out of phase (Figures 2a and 3a). Since a steeper lapse rate is associated to a smaller water storage capacity of the atmosphere, this result shows that, while it involves actually all seasonal shape change of the temperature profile, $\Delta^\Gamma W$ is mostly sensitive to the mass-weighted lapse rate. In high latitudes, the lapse rate being minimum during summer, it reinforces the seasonal amplitude of W. The seasonal lag between the SST and Γ certainly explains the small lag between the SST and the precipitable water (Figure 2a).

In view of these results, one may conclude that the seasonal variation of g_s (that is, the greenhouse effect related to the total atmospheric transmittance; see section 2) due to W is not only related to seasonal SST variations but also to variations of the relative humidity profiles (mainly in the tropics) and of the temperature lapse rate (mainly in middle and high latitudes). The following section will combine this result to greenhouse effect observations in order to highlight the relative role of the LW atmospheric opacity (g_s) and the atmospheric emission to space (e_a) in the seasonal variation of the clear-sky greenhouse effect.

Seasonal Variations of the Clear-Sky Greenhouse Effect (g_c)

The annual mean distribution of g_c for 1988 in given q_{s_o} intervals (Figure 1b) exhibits the well-known increase of g_c with the SST [*Raval and Ramanathan,* 1989; *Stephens and Greenwald,* 1991; *Duvel and Bréon,* 1991]. The standard deviation of g_c mixes the effects of both geographical and seasonal variations of the greenhouse effect. These variations, together with the mean slope of g_c, may be perturbed by systematic changes of the vertical structure of the troposphere with latitude or season. For example, the progressive increase of the lapse rate with the SST (Figure 1a) acts to increase the g_c-SST slope. Also, the larger standard deviation of the lapse rate for cold regions corresponds to the larger standard deviation of g_c. In the present section we analyze in more detail the role of the vertical structure on the seasonal variability of the clear-sky greenhouse effect.

The greenhouse seasonal phase (Figure 2a) exhibits a progressive shift from summer in the tropics to winter in high latitudes. Over middle and high latitudes, the seasonal variation of g_c is thus not in phase with the SST or the precipitable water. This striking result demonstrates that the seasonal variation of g_c over particular regions is not primarily related to variations of the total atmospheric transmittance but rather to variations of the atmospheric infrared emission to space (e_a). In a first approach, the influence of the lapse rate (and thus e_a) on the seasonal variation of g_c is strongly sug-

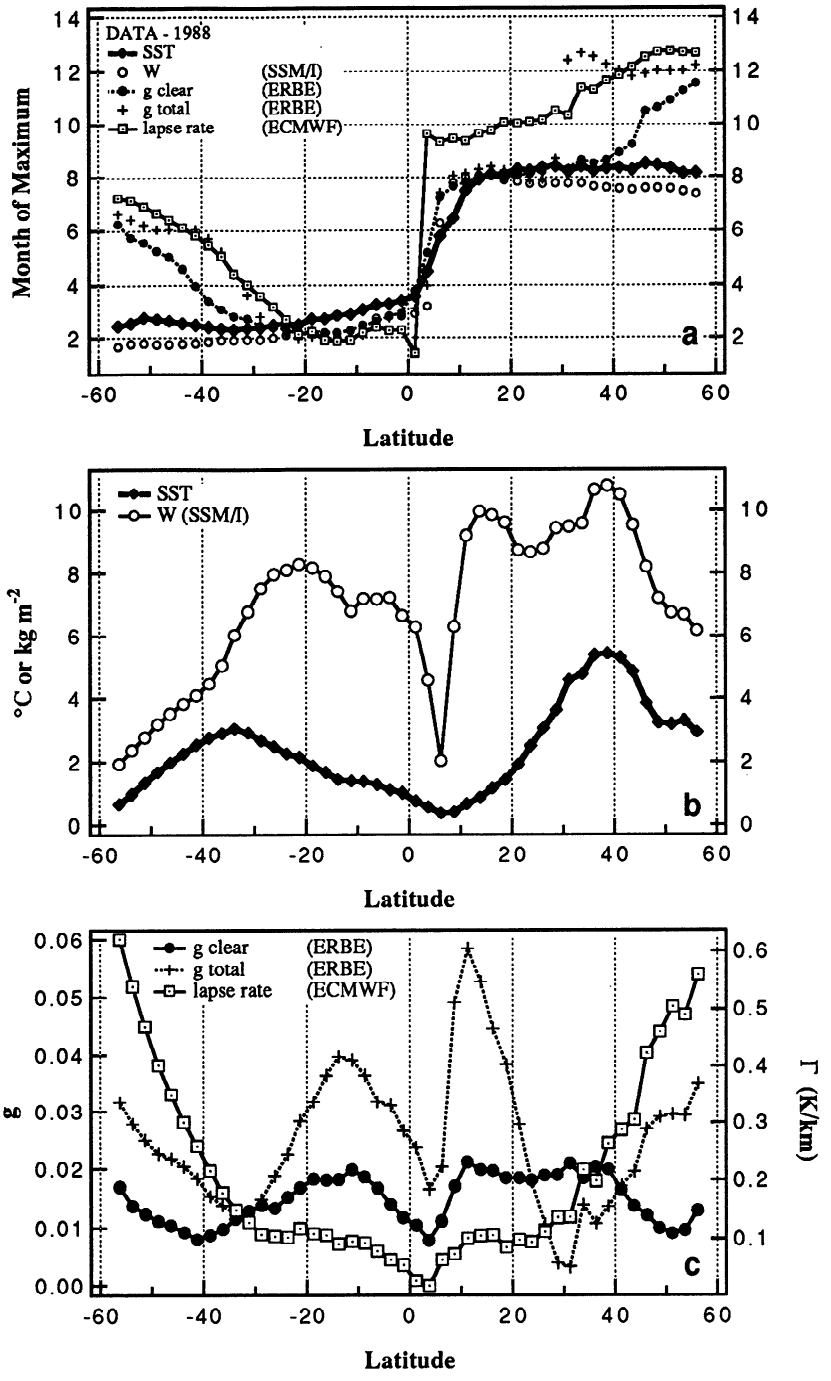

Figure 2. (a) Phase of the first harmonic of the zonally averaged seasonal variation of the SST, precipitable water (W), clear-sky and total greenhouse effect and of the temperature lapse rate. The seasonal phase is expressed here as the month of maximum. (b) Amplitude of the first harmonic of the zonally averaged seasonal variation of the SST and precipitable water. (c) Amplitude of the first harmonic of the zonally averaged seasonal variation of the clear-sky and total greenhouse effect and of the temperature lapse rate. All variables are derived from satellite data or ECMWF analyses over ocean regions for the year 1988.

gested by the similar progressive shift of their phases from tropics to high latitudes.

In clear-sky conditions and for a given columnar water vapor amount, a large atmospheric LW emission may be produced either (1) by a small mean tropospheric lapse rate ($\Gamma = -dT/dz$) or (2) by relatively dry upper tropospheric layers compared to lower layers. In order to assess the relative importance of these two processes, we compute the mean clear-sky greenhouse effect in given intervals of both precipitable water and SST (or q_{s_o}). This is shown on Figure 4 for winter and summer and for the northern hemisphere only. Although W

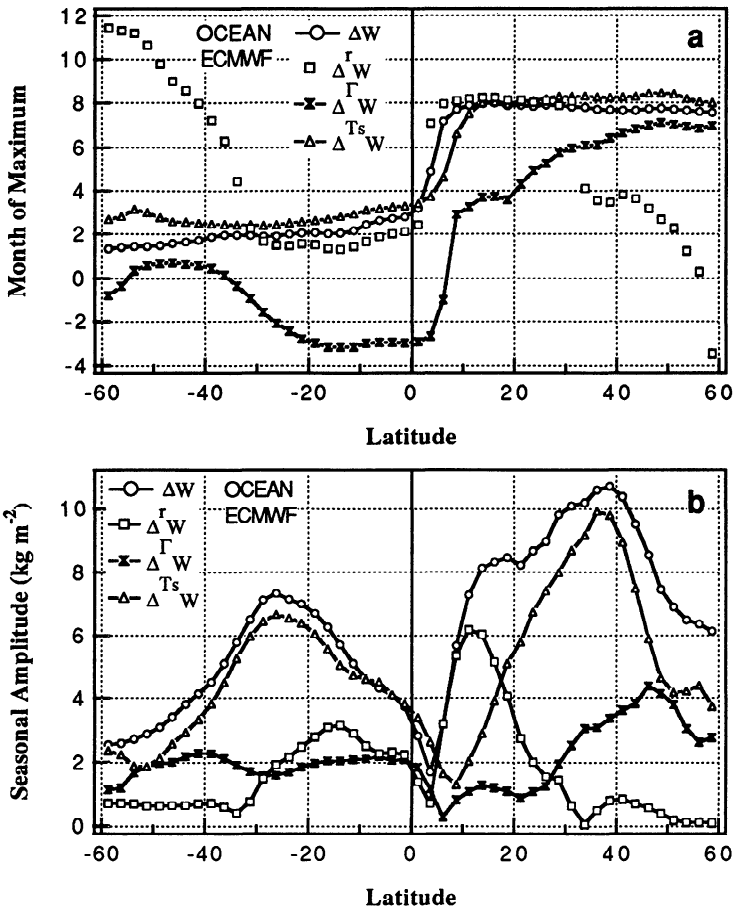

Figure 3. Latitudinal distribution of (a) the seasonal phase (expressed as the month of maximum precipitable water produced by a given component) and (b) amplitude of the different components of the precipitable water variations derived from ECMWF analyses. ΔW refers to actual precipitable water variations, while Δ^rW, Δ^{Ts}W and Δ^ΓW refer to precipitable water changes associated to relative humidity profile variations, vertically uniform temperature variations, and temperature lapse rate variations, respectively (see text).

and q_{s_o} intervals are fixed, the summer and the winter distributions are very different. During winter the variation of g_c as a function of W presents nearly the same slope for the different q_{s_o} intervals. On the contrary, the summer distribution is very different with slopes even becoming negative for q_{s_o} <12 g/kg (SST<17°C). In addition, for a given W, the clear-sky greenhouse effect is larger for larger SST. This tends to demonstrate that, for the northern hemisphere ocean, the geographical distribution of the vertical atmospheric structure is far more variable during summer than during winter and that, besides its dependence on the columnar water vapor amount, the greenhouse effect strongly depends on this vertical structure.

This systematic variation of the mean greenhouse effect may reflect forced variations of humidity profiles with W and the SST. However, the relative humidity near the ocean surface being quite constant [*Prabhakara et al.*, 1979], the surface humidity over ocean is roughly proportional to q_{s_o}. For a constant precipitable water, less water vapor is expected in altitude for larger q_{s_o}. Considering that a smaller amount of water in altitude tends to decrease the greenhouse effect, the greenhouse effect at constant W should be smaller for larger SST (q_{s_o}) [*Duvel et al.*, 1993]. Also, the greenhouse effect should obviously increase with W, and faster at constant q_{s_o} because more water is expected in altitude. A strong compensating effect must thus exist to explain the observed distributions during NH summer, i.e., the increase of the greenhouse effect with q_{s_o} at constant W and the negative slopes of the g_c-W relation for cold regions.

The influence of the vertical temperature lapse rate on the distribution of the greenhouse effect is studied by using monthly mean temperature profiles from ECMWF analyses (see section 2). Computing the mean lapse rate in the same q_{s_o}-W intervals highlights a striking correspondence between the distributions of Γ_m and g_c for NH, during both summer and winter (Figure 4). The g_c distribution appears to be driven by systematic variations of the vertical temperature structure with W and the SST, i.e., (1) for SST<17°C, a smaller lapse rate (smaller temperature decrease with height) for a larger W at constant q_{s_o}; (2) for a given W, a smaller lapse

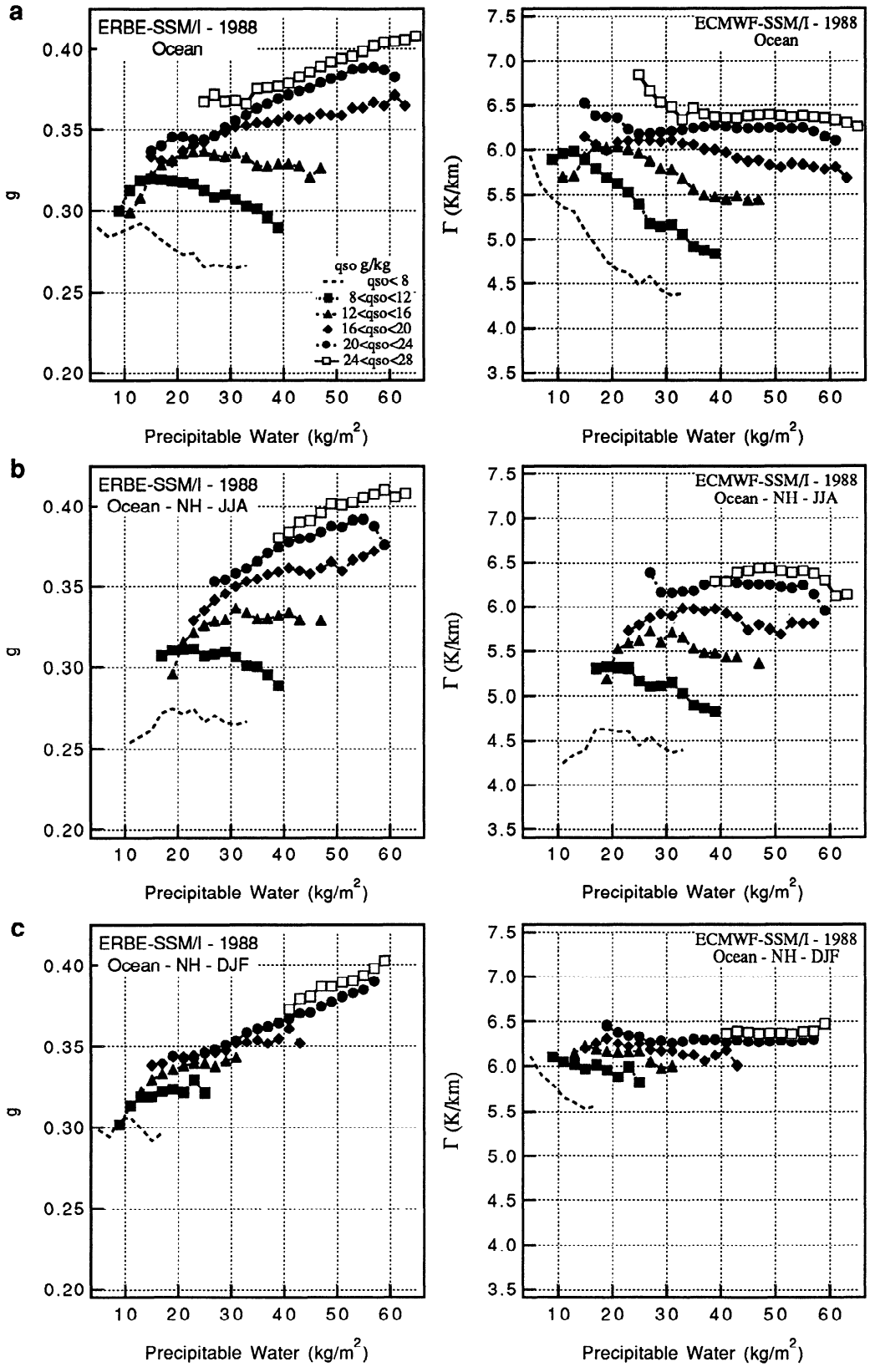

Figure 4. Mean relations between (left) the clear-sky greenhouse effect and the precipitable water or (right) between the mass-weighted lapse rate and the precipitable water in regular intervals of surface saturation humidity q_{so} (in grams per kilogram) computed from regional monthly means over ocean. (a) Over global ocean when considering the whole year 1988; (b) for northern hemisphere in summer (June-July-August); (c) for NH in winter (December-January-February).

rate for colder regions and (3) by comparing summer and winter results, a stronger lapse rate during winter than during summer in middle and high latitudes. In the tropics, the lapse rate is always close to the moist adiabatic value and only weakly variable. The variation of the precipitable water at constant q_{s_o} is thus mainly related to change in the relative humidity in altitude, explaining the strong increase of g_c with the precipitable water in the tropics (Figure 4) in agreement with *Hallberg and Inamdar* [1993].

These tendencies remain while considering global ocean for all months (Figure 4). This suggests that the above behavior is a strong characteristic of the thermodynamical structure of the troposphere. In fact, a large precipitable water for a relatively cold surface can be obtained only with more water in altitude and thus with a small lapse rate to avoid supersaturation. Concerning the seasonal variation over middle and high latitude ocean, present results demonstrate that the negative effect of the lapse rate on the greenhouse effect, due to the increase in atmospheric emission (e_a), is stronger than its positive effect due to the larger W (and thus g_s).

4. The Observed Seasonal Cycle Over Land Regions

Since there is no SSM/I estimate of the precipitable water over land, we use the precipitable water derived from ECMWF analyses. However, since there are far more conventional meteorological stations over land compared to ocean, the ECMWF estimates of W are also certainly more reliable over land, especially for northern middle latitudes. Land surface temperatures (LST) considered are estimates reported in the ISCCP C2 data set. These LST are actually estimates of the surface blackbody temperature in the atmospheric window (i.e., 10-12 μm) and are not corrected for longwave surface emissivity [*Rossow and Garder,* 1993]. To compute g_c, we thus simply estimate the longwave radiation emitted by land surfaces as the blackbody value σT_s^4.

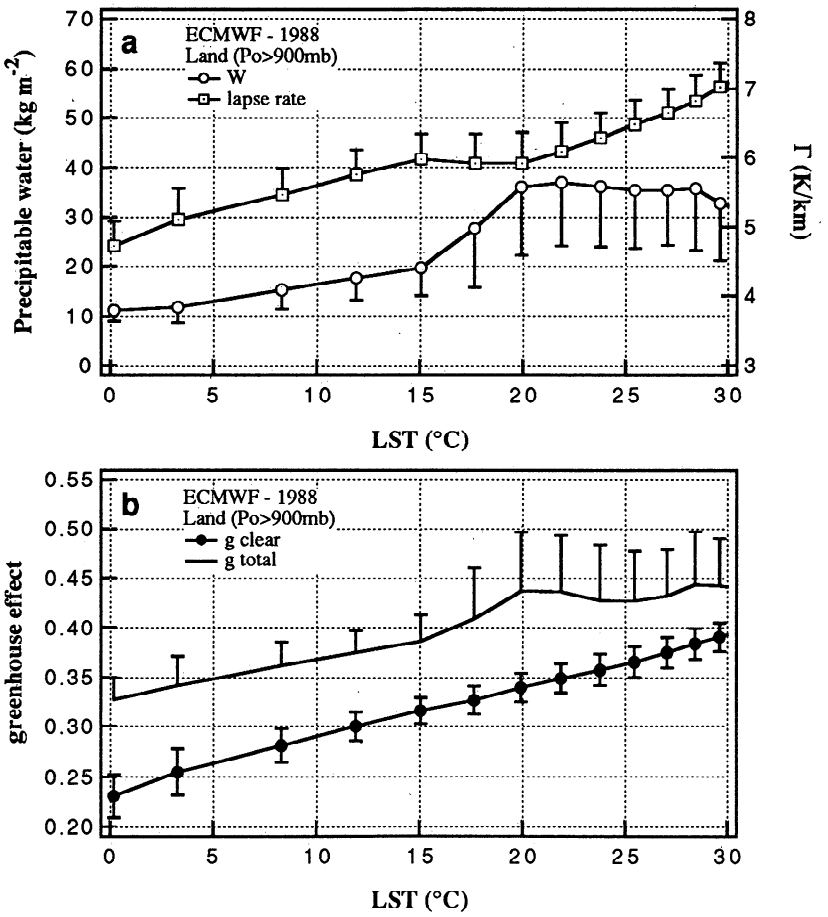

Figure 5. (a) Mean precipitable water and mass-weighted tropospheric lapse rate over land derived from ECMWF analyses averaged in different land surface temperature (LST) intervals. Only land regions for which surface pressure exceeds 900 mbar are considered. Vertical bars indicate the half standard deviation within each saturation specific humidity interval. (b) Same as Figure 5a but for the clear-sky and total components of the normalized greenhouse effect derived from ERBE data over land. Land surface temperatures estimates for the year 1988 are derived from ISCCP data.

To avoid spurious results due to the variable topography, we have considered only land regions with a surface pressure larger than 900 mbar. However, we have observed that the consideration of all land regions does not significantly modify the zonal mean results, so that present results can be considered as representative of a mean behavior for all land regions.

Seasonal Variations of the Precipitable Water

As for ocean regions, there is a stronger scatter of the precipitable water over warm tropical regions (Figure 5). It is also worth noting that, while the precipitable water increases regularly from cold to warm region over ocean, the average W over land exhibits a steep increase for LST between 15° and 20°C and remains nearly constant above with a large standard deviation of the order of 15 kg/m^2. The large variability of the atmospheric vertical structure over tropical land (for a given surface temperature) is possibly because the vertical structure of the atmosphere is more determined by monsoon activity than by the local surface temperature. Moreover, the variability of the lapse rate is larger over land (Figure 5a) than over ocean (Figure 1a) leading to a larger variability of water storage of the atmosphere. Finally, a fundamental difference between land and ocean regions is that water vapor and cloud have a strong direct radiative impact on the local surface temperature over land because of the smaller thermal inertia of the ground.

The seasonal phase of W is very close to the LST phase poleward of 20° and exhibits a large lag of approximately 4 months in the tropics (Figure 6a). This phase lag may be also attributed to the monsoon activity that increases the precipitable water and decreases the surface temperature because of enhanced evaporation and radiative cooling effect of high convective clouds. As for ocean, the relative humidity over tropical land regions is the main driving factor for the seasonal variation of the precipitable water (Figure 7). In middle latitudes, while the seasonal amplitude of the surface temperature is 3 times larger over land (Figure 6b) compared to ocean (Figure 2b), the amplitude of W is of the same order (i.e., around 10 kg/m^2). This is because, poleward of roughly 25°, seasonal variations of relative humidity and lapse rate act to reduce the large seasonal amplitude of the precipitable water ($\Delta^{T_s}W$) related to the large seasonal variation of the surface temperature (Figure 7). The seasonal amplitude of the lapse rate over land (Figure 6c), twice as large compared to ocean (Figure 2c), tends to decrease the seasonal amplitude of W by roughly 7 kg/m^2 ($\Delta^{\Gamma}W$ on Figure 7). This is because a smaller lapse rate during winter increases the water storage capacity in altitude and thus the precipitable water. Relative humidity variations ($\Delta^{r}W$) also tend to increase W in winter (Figure 7a) with, however, a very small amplitude (Figure 7b).

Seasonal Variations of the Clear-Sky Greenhouse Effect

Despite the nearly constant W for a LST>20°C, g_c progressively increases with the surface temperature (Figure 5b) in accordance with the increase of the mass-weighted lapse rate that tends to increase g_c and decrease W. In middle and high latitudes, the preponderance of $\Delta^{T_s}W$ on the seasonal variation of W (Figure 7) and the close agreement between both seasonal phase and amplitude of the LST and Γ (Figure 6) give a seasonal variation of g_c in phase with the LST. These three parameters (LST, Γ and g_c) have an amplitude that progressively increases toward high latitudes up to roughly 40°. The in-phase relation between W and Γ gives a large seasonal amplitude of the clear-sky greenhouse effect (4 times larger than over ocean at 30°S or 40°N). In the tropics, the seasonal amplitude of g_c is weaker than over middle latitudes despite the stronger variation of the precipitable water (Figure 6). This is because the seasonal variation of the precipitable water is mainly driven by the relative humidity (Figure 7) and has a strong phase lag relative to Γ.

The global and annual distributions of g_c and Γ in the different q_{s_o}-W intervals are presented on Figure 8. For land regions, the distributions for NH-summer and NH-winter are both very similar to this global annual distribution and are thus not displayed. Compared to ocean regions, there is thus a far more robust relation between the LST and the mean lapse rate (especially in middle and high latitudes) that also gives a more robust relation between the LST and the greenhouse effect. The increase of the mean lapse rate with surface temperature is independent of the W interval considered and gives a stronger greenhouse effect for warmer regions. Except for the lowest q_{s_o} interval (i.e., q_{s_o}<8 g/kg), the slopes of g-W (or Γ-W) also are similar for all q_{s_o} intervals. In each q_{s_o} (or LST) interval, larger precipitable water corresponds to smaller lapse rates, that can be easily understood since a smaller lapse rate allows more water to be stored in altitude. There is thus a compensating effect between the larger g_s due to the larger W and the larger e_a due to the smaller lapse rate. This gives a nearly constant greenhouse effect for W between 15 and 40 kg/m^2 for most LST intervals.

In the tropics, the most striking difference with regard to ocean regions is the strong increase of the mean lapse rate as a function of the LST, even for dry regions. The strongest greenhouse effect in warmer regions is thus not related to largest W but to largest lapse rates. Over land, these regions correspond to desert area during summer.

5. Impact of the Cloudiness

This section evaluates the role of cloudiness in perturbing the observed seasonal variation of the clear-sky greenhouse effect. On the average, cloudiness perturbs the greenhouse effect by about 25% (Figures 1b and 5b). However, the standard deviation of g is generally much larger than the standard deviation of g_c. Despite their relatively weak contribution on the annual mean greenhouse effect, clouds thus play a fundamental role in the spatio-temporal variability of the radiation field at the top of the atmosphere. It is worth noting that

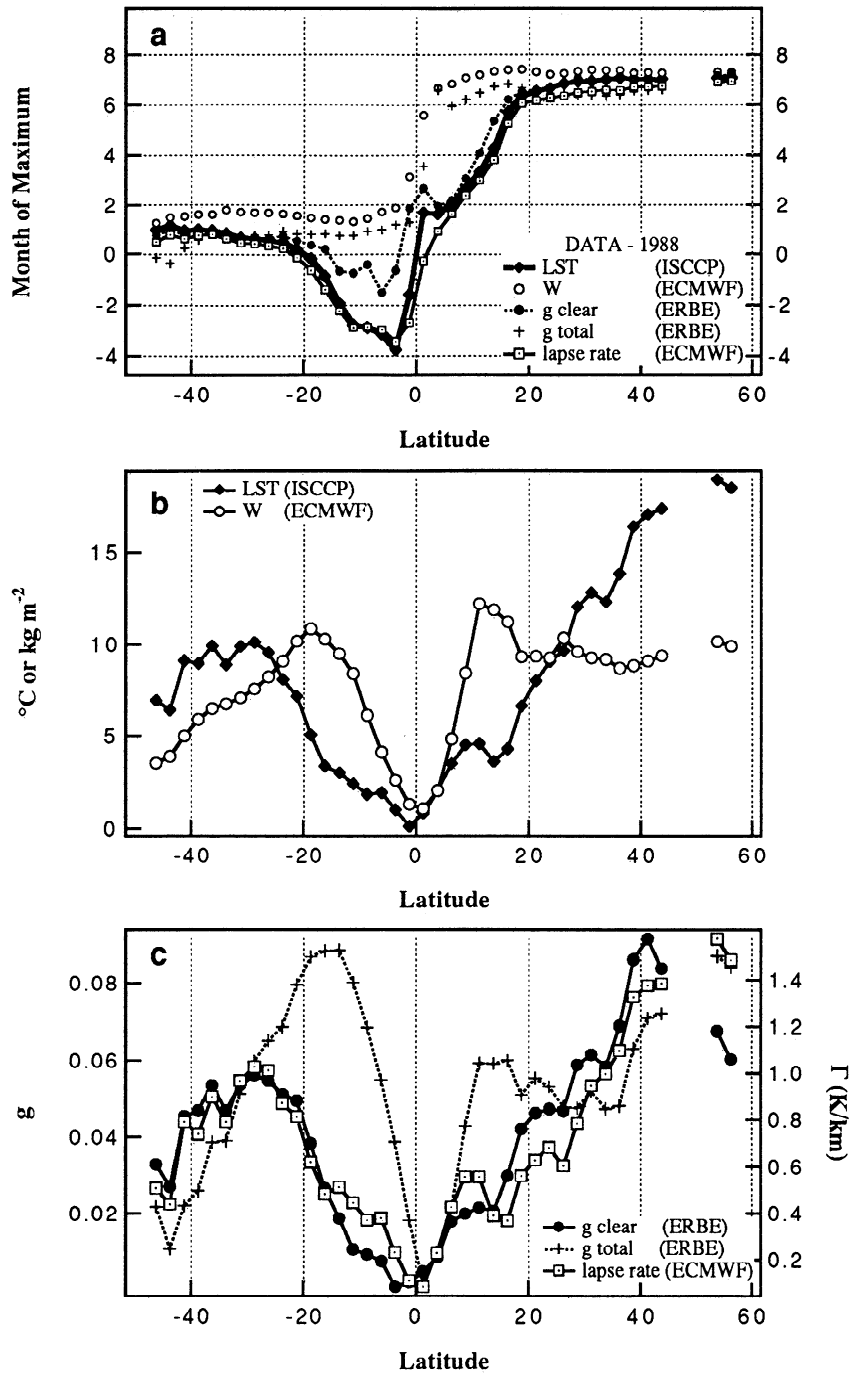

Figure 6. Same as Figure 2 but for land regions.

the mean g remains nearly constant for SST between 15° and 25°C over ocean and for LST larger than 20°C over land (as for W).

Over ocean, the total greenhouse effect (g) is in phase with the SST up to 30° and lags the SST by 4 months poleward (Figure 2). The phase lag between g and g_c exceeds 2 months only around 30°N. The amplitude of g is generally larger than the amplitude of g_c, except around 30° where g has a large phase jump that reduces locally the coherence of the seasonal variation. The most striking impact of cloudiness occurs in the tropics where clouds increase threefold the seasonal amplitude of the greenhouse effect. Clouds also increase this amplitude poleward of 40°. Over land regions (Figure 6), clouds strongly increase the seasonal amplitude of the greenhouse effect in the tropics and slightly decrease this amplitude poleward of 30°.

For both land and ocean regions, the seasonal impact (phase and amplitude) of cloudiness on the greenhouse effect appears mainly to be linked to precipitable water over the tropics (and thus to the relative humidity) and to the lapse rate over middle and high latitudes. The found influence of the lapse rate on the cloud-induced greenhouse effect can be justified since a larger lapse

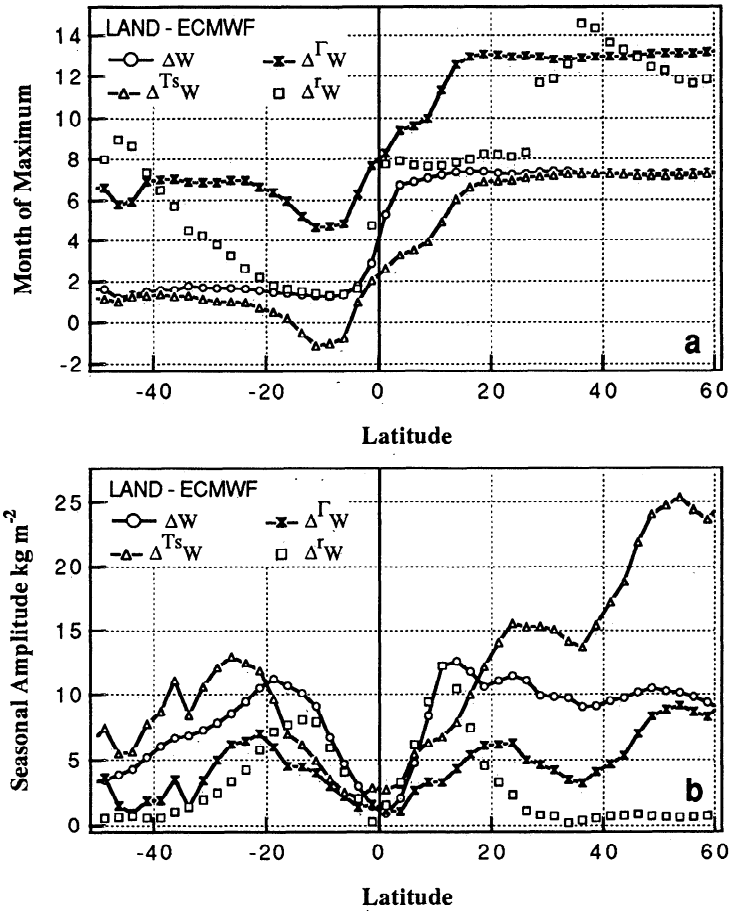

Figure 7. Same as Figure 3 but for land regions.

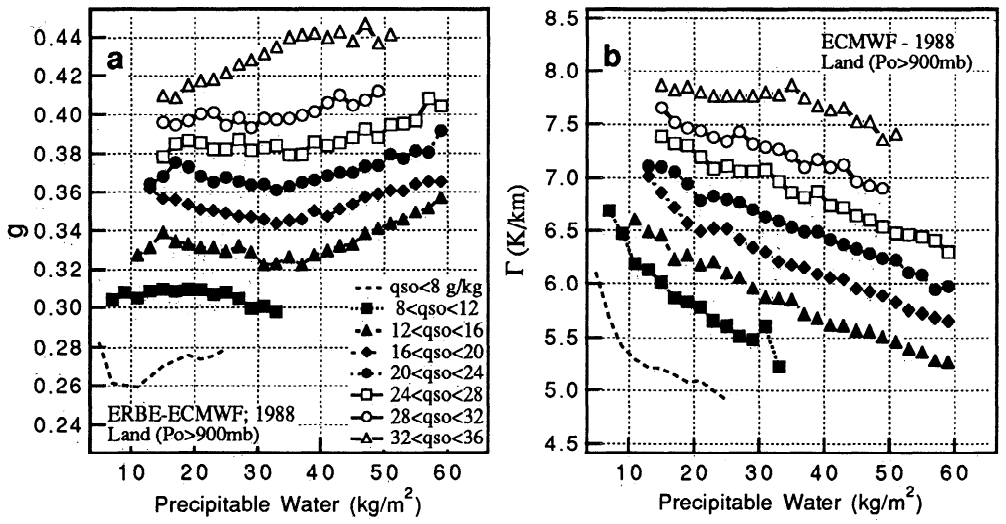

Figure 8. Mean relations (a) between the normalized clear-sky greenhouse effect g (derived from ERBE data) and the precipitable water and (b) between the mass-weighted lapse rate Γ and the precipitable water for different intervals of surface saturation humidity q_{so} (in grams per kilogram). These relations are computed from regional monthly means over land for the year 1988.

rate means a more unstable atmosphere and a stronger temperature contrast between the cloud top and the surface. In high latitudes, the lapse rate thus tends to maximize both clear and total greenhouse effect in winter.

6. LMD-GCM Evaluation and Analysis

This section presents briefly an application of above results to the evaluation of general circulation models. We use the LMD (Laboratoire de Météorologie dynamique) GCM, a grid-point model discretized regularly in longitude (64 points), in sine of latitude (50 points) and irregularly along the vertical (11 sigma levels). Main characteristics of this GCM are described in detail by *Sadourny and Laval* [1984], *Le treut and Li* [1991] and by *Bony et al.* [1992]. Concerning the water budget, the model contains a supersaturation scheme on which the parameterization of nonconvective cloudiness is based, a Kuo scheme and a moist adiabatic adjustment scheme for the representation of penetrative cumulus convection. No diurnal forcing is applied. The longwave radiation code is the scheme originally developed by *Morcrette et al.* [1986] and recently updated *Morcrette* [1990]. The parameterization of the water vapor continuum used in the Morcrette code is an empirical formulation originally developed by *Roberts et al.* [1976] and using coefficients derived from *Clough et al.* [1980].

We analyze the last year of a 10-year (1979-1988) simulation forced with observed SST and sea-ice distributions. The LMD-GCM is also used to get some quantitative arguments on the relative role of temperature and moisture vertical structures on the seasonal variation of the greenhouse effect. Considering model output for the year 1988, we have performed off-line radiative computations of the monthly mean clear-sky longwave radiation with modified temperature and humidity profiles. Because of the nonlinear dependence of LW fluxes on temperature and humidity conditions, the clear-sky greenhouse effect computed on the basis of monthly mean atmospheric profiles is likely to differ from that computed at each time step in the model. In fact, despite a slight underestimate of the seasonal amplitude of the clear-sky greenhouse effect by about 6% over ocean (and negligible over land), time averaging of the atmospheric profiles does not affect the seasonal phase of the greenhouse effect.

The seasonal phase of the precipitable water (Figure 9a) over ocean is in very close agreement with observation (Figure 2). However, the simulated seasonal amplitude is underestimated, especially in the northern hemisphere (Figure 9b). The source of this discrepancy is analysed by using the method described in section 2

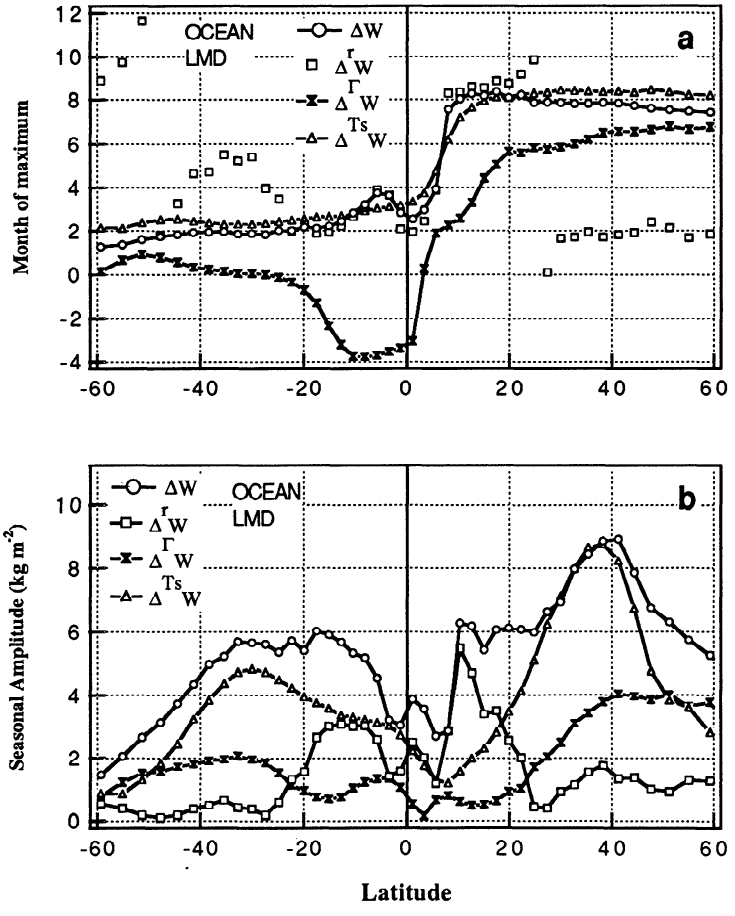

Figure 9. Same as Figure 3 but for LMD GCM simulations.

(equations (3)-(9)). One may first note that the simulated origin of the water vapor seasonal variation is in general agreement with the ECMWF analyses (Figure 3). Surprisingly, a large part of the amplitude discrepancy is due to the influence of uniform temperature change (i.e., $\Delta^{T_s}W$) that is smaller in the LMD-GCM simulation (Figure 9b). This highlights bias in the simulated mean vertical structure. Particularly, in agreement with *Boer et al.* [1992] who pointed out a cold bias in the upper troposphere, the mass-weighted lapse rate is too large in the model, giving a smaller impact of uniform temperature change on precipitable water. Other sources of disagreement also appear, such as the underestimate of the amplitude of $\Delta^{r}W$ between 10°N and 20°N. Also, around 40°N, the seasonal amplitude of W is reduced because the phase of $\Delta^{r}W$ is not well simulated (out of phase with the SST) and its amplitude is too strong.

Over ocean, the latitudinal distribution of the seasonal phase and amplitude of the greenhouse effect is relatively well reproduced by the LMD-GCM (Figure 10). The main discrepancy compared to ERBE observations (Figure 2) is the lower seasonal amplitude partly due to the computation method (i.e., use of monthly mean) but also certainly to the too small seasonal amplitude of W. The influence of temperature variations on the seasonal greenhouse effect is analyzed by fixing for each region the relative humidity profile at its annual mean value. To investigate the role of seasonal change of the temperature profile shape on g_c we compute g_c considering only uniform seasonal temperature variations (the relative humidity is fixed but the water vapor varies with the saturation water vapor). In the tropics, the relative humidity is clearly the main driving factor for the modeled seasonal variation of g_c. As for the precipitable water, the underestimated seasonal amplitude of g_c in the tropics may thus be attributed to the too small seasonal variation of the zonal-mean relative humidity in the LMD-GCM. In middle latitudes, the phase of g_c is only slightly affected when the relative humidity is held constant. However, around 40°N, since the mean relative humidity is maximum during winter, the amplitude of g_c is enhanced. When the vertical temperature structure is held constant, the phase of g_c is strongly affected (Figure 10a). This highlights the lapse rate influence on the seasonal phase of g_c.

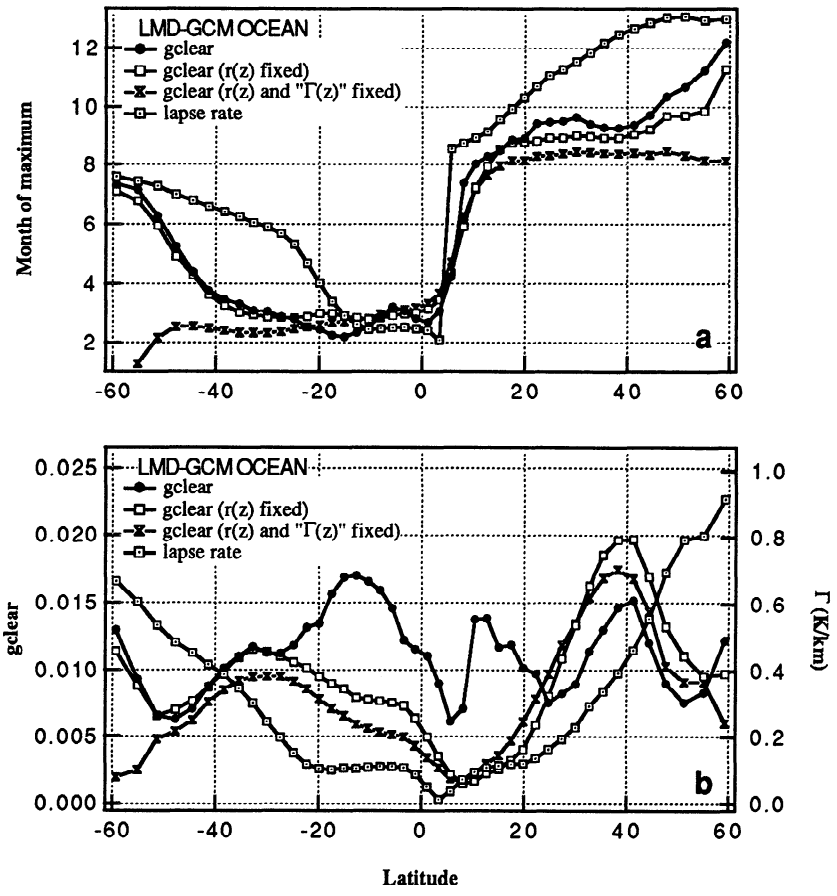

Figure 10. Latitudinal distribution of (a) the seasonal phase and (b) amplitude of the clear-sky greenhouse effect actually computed by the LMD GCM over the ocean, and that computed (through off-line radiative computations) when regional monthly mean values of relative humidity profiles ($r(z)$) or relative humidity profiles and lapse rates ($\Gamma(z)$) are fixed and set to their annual mean values. Also reported is the seasonal phase and amplitude of the simulated mean tropospheric mass-weighted lapse rate over ocean.

Since the seasonal amplitude of the lapse rate over NH middle latitude is stronger in the LMD-GCM (Figure 10) compared to ECMWF analyses (Figure 2), the too small simulated seasonal variation of g_c may be mostly attributed to the too small seasonal amplitude of W.

Concerning the seasonal variation of the precipitable water over land, the main discrepancy between the LMD-GCM and ECMWF analyses is the larger simulated seasonal amplitude in the tropics (Figure 11). This is related to a larger amplitude of $\Delta^r W$ in the LMD-GCM. In mid-latitudes, the LMD-GCM seasonal amplitude of W is very close to that of the ECMWF analyses while there are some compensating effects between $\Delta^r W$ (too large), $\Delta^\Gamma W$ (too small) and $\Delta^{T_s} W$. Concerning the greenhouse effect, the LMD-GCM simulation well reproduces the phase of the seasonal variation and again underestimates slightly the seasonal amplitude. As for ocean regions, we use the LMD-GCM to quantify the influence of temperature and humidity profiles on the seasonal variation of the greenhouse effect (Figure 12). Because LST and Γ_m vary in phase and because W is mainly driven by the seasonal variation of the LST, fixing either the relative humidity or the lapse rate does not modify the phase of the greenhouse effect (not shown). For middle and high latitudes, fixing the relative humidity increases the seasonal amplitude of W and thus the amplitude of the greenhouse effect (Figures 11 and 12). At these latitudes, the too small simulated seasonal amplitude of g_c is thus certainly due to the too strong seasonal variation of the mean relative humidity. Fixing the lapse rate decreases the greenhouse effect in summer and thus decreases the seasonal amplitude of the greenhouse effect. In the tropics, both relative humidity and lapse rate variations tend to increase the seasonal amplitude of the greenhouse effect.

7. Summary and Discussion

We have analyzed observed seasonal variations of precipitable water and greenhouse effect over ocean and land regions. Throughout the analysis, we have tried to isolate the different contributions of water vapor and temperature vertical distributions on the greenhouse effect. This includes (1) the influence of the vertical profiles of relative humidity and temperature on the precipitable water and thus on the total atmospheric transmittance and (2) the influence of these vertical distributions on the atmospheric emission to space. Results show that the nature and the origin of the seasonal variation of the greenhouse effect strongly depend on the area of the globe considered.

Over middle and high latitude ocean, especially in the northern hemisphere, the radiative effect of the temperature lapse rate dominates the seasonal variation of the

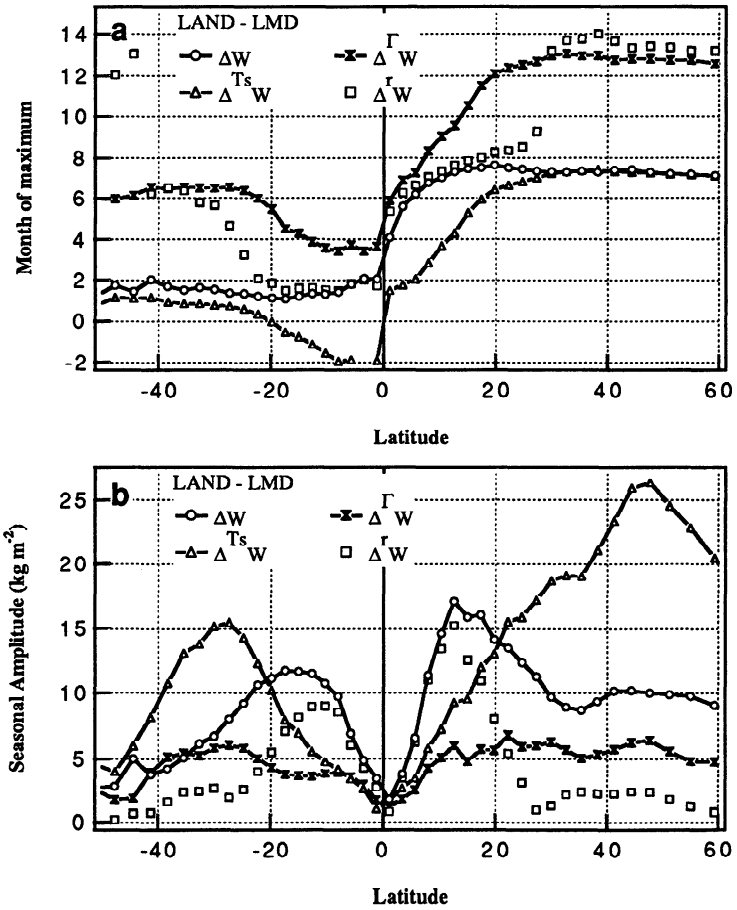

Figure 11. Same as Figure 9 but for land regions.

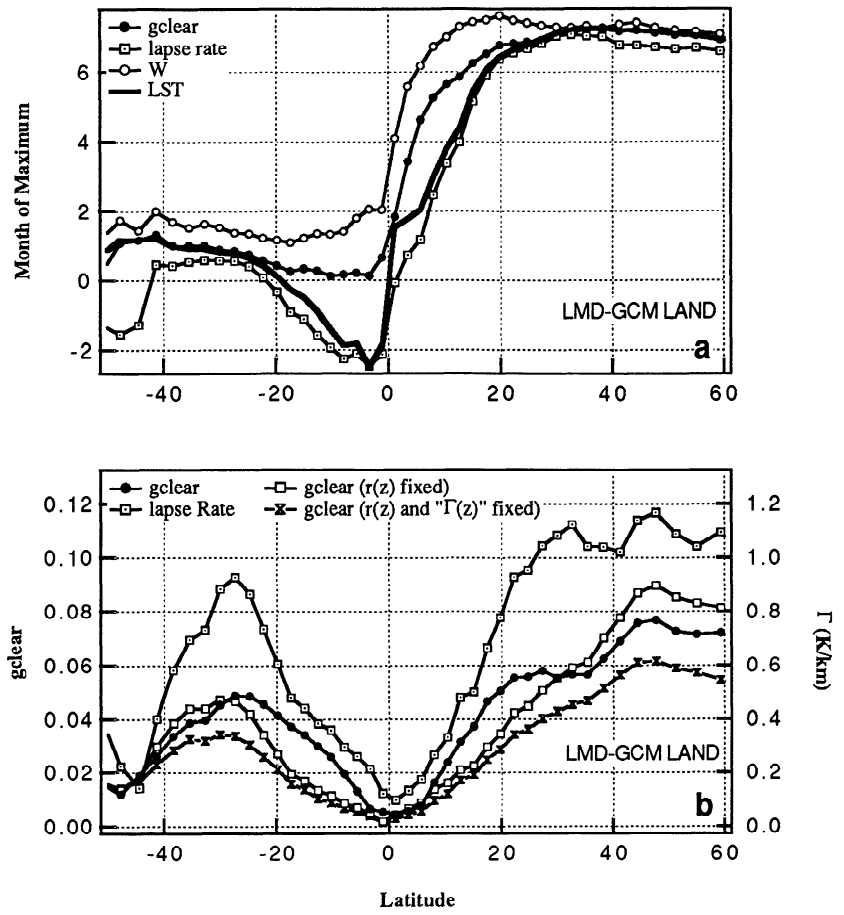

Figure 12. (a) Phase of the first harmonic (expressed as the month of maximum) of the zonally averaged seasonal variation of the clear-sky greenhouse effect, temperature lapse rate, precipitable water and surface temperature (LST) simulated by the LMD GCM over land regions. (b) Amplitude of the zonally averaged seasonal variation of the clear-sky greenhouse effect actually computed by the LMD GCM over land regions, and that computed when regional monthly mean values of relative humidity profiles or relative humidity profiles and lapse rates are fixed and set to their annual mean values. Also reported is the seasonal phase and amplitude of the simulated mass-weighted lapse rate over land regions.

greenhouse effect and leads to large seasonal phase lags between the precipitable water and the greenhouse effect, with even a phase opposition for high latitudes, in agreement with *Webb et al.* [1993]. Over middle latitude ocean, present results demonstrate that the negative effect of the lapse rate on the greenhouse effect due to the increase atmospheric emission (e_a) is stronger than its positive effect due to both larger W (and thus g_s) and larger amount of water in altitude. The general behavior is, however, relatively hard to apprehend because the different parameters influencing the precipitable water and the greenhouse effect (i.e., surface temperature, relative humidity and temperature lapse rate) do not vary with the same seasonal phase for a given latitude and do not have constant phase for the different latitudes. For northern hemisphere land regions, the seasonal variations of relative humidity and lapse rate act to reduce the large seasonal amplitude of the precipitable water related to the large seasonal variation of the surface temperature. The seasonal amplitude of the clear-sky greenhouse effect is enhanced by lapse rate variations (despite its action on the precipitable water) and reduced by relative humidity variations. The larger lapse rate during summer over land and during winter over ocean is in accordance with *Gulev et al.* [1991] who pointed out, on the basis of monthly mean temperature data over the period 1957-1971, a positive correlation between the monthly averaged tropospheric lapse rate and surface temperature over land, and negative correlation over ocean. Note that the larger land mass in the NH may explain the stronger seasonal amplitude of the lapse rate over NH compared to SH ocean but is certainly not sufficient to explain the progressive latitudinal shift of its seasonal phase. This is because the phase of both observed and modeled greenhouse effect is very similar for the 2 hemispheres. Further study is needed to understand fully the origin of the seasonal behavior of the temperature lapse rate over middle latitude ocean.

Over tropical regions, the seasonal variation of the

relative humidity strongly influences the seasonal variation of both precipitable water and greenhouse effect. For these regions, lapse rate variations are small and it is the total atmospheric transmittance that mainly drives the seasonal variation of the clear-sky greenhouse effect. Over land, the monsoon activity leads to a seasonal phase lag of roughly 2 months relative to the surface temperature.

We have shown that the vertical structure of the troposphere strongly influences the seasonal variation of clear-sky and total greenhouse effect. Despite the very variable origin of such an influence, we have tried to extract some elements of simplicity that explain systematic aspects of the relation between the surface temperature, the precipitable water and the greenhouse effect. We have used the LMD-GCM to give a possible application of above results for the evaluation of general circulation models. The LMD GCM simulation of the seasonal cycle of both precipitable water and greenhouse effect is in general agreement with observation. Main discrepancies are due to a too large impact of the seasonal variation of the mean relative humidity (except over tropical ocean) and to a too large annual mean temperature lapse rate over ocean. This highlights bias in the model response to an external forcing due not only to the response of the different physical parameterizations but also to the model description of the mean atmospheric state. The understanding of the origin of these discrepancies requires, however, more detailed analyses and the consideration of other GCMs. This also requires more work to understand the precise origin of the obseved seasonal variation of the vertical structure of the atmosphere. Finally, better knowledge of the impact of the variability of the atmospheric structure on the radiative equilibrium of the Earth requires the examination of other types of observable variations and the evaluation of the model description of these variations. A study of interannual changes is in progress at LMD and will be reported in a future paper.

Acknowledgments. The present work was supported in part by the French Ministère de la Recherche et de la Technologie. The authors thank Hervé Le Treut for his valuable suggestions, Ali Harzallah who performed the LMD GCM simulations, and R. S. Kandel, and J.-J. Morcrette for their useful comments about the manuscript.

References

Arpe, K., The hydrological cycle in the ECMWF short range forecasts., paper presented at the ECMWF workshop, Eur. Cent. for Medium-Range Weather Forecasts, Reading, England, November 1990.

Barkstrom, B. R., The Earth Radiation Budget Experiment (ERBE), *Bull. Am. Meteorol. Soc.*, *65*, 1170–1185, 1984.

Barkstrom, B. R., E. F. Harrison, G. L. Smith, R. Green, J. Kibler, R. Cess, and the ERBE Science Team, Earth Radiation Budget Experiment (ERBE) archival and April 1985 results., *Bull. Am. Meteorol. Soc.*, *70*, 1254–1262, 1989.

Boer, G. J., et al., Some results from an intercomparison of the climates simulated by 14 atmospheric general circulation models., *J. Geophys. Res.*, *97*, 12,771–12,786, 1992.

Bony, S., H. Le Treut, J.-P. Duvel, and R. S. Kandel, Satellite validation of GCM-simulated annual cycle of the Earth Radiation Budget and cloud forcing, *J. Geophys. Res.*, *97*, 18,061–18,081, 1992.

Cess, R. D., et al., Intercomparison and interpretation of climate feedback processes in 19 atmospheric general circulation models., *J. Geophys. Res.*, *95*, 16,601–16,615, 1990.

Clough, S. A., F. X. Kneizys, R. Davies, R. Gamache, and R. Tipping, Theoretical line shape for H_2O: Application to the continuum, in *Atmospheric Water Vapour Absorption*, edited by A. Deepak, T. D. Wilkerson and L. H. Ruhnke, pp. 25–46, Academic, San Diego, Calif., 1980.

Duvel, J. P., and F. M. Bréon, The clear-sky greenhouse effect sensitivity to a sea surface temperature change, *J. Clim.*, *4*, 1162–1169, 1991.

Duvel, J.-P., R. S. Kandel, S. Bony, and H. Le Treut, Relation between the precipitable water and the greenhouse effect: Lapse rate influence, in *IRS'92: Current Problems in Atmospheric Radiation*, edited by S. Keevallik and O. Karner, A. Deepack publishing, pp. 158–162, Tallin, Estonia, 1993.

Esbensen, S. K., D. B. Chelton, D. Vickers, and J. Sun, An analysis of errors in special sensor microwave imager evaporation estimates over the global oceans, *J. Geophys. Res.*, *98*, 7081–7101, 1993.

Gaffen, D. J., W. P. Elliott, and A. Robock, Relationships between tropospheric water vapor and surface temperature as observed by radiosondes, *Geophys. Res. Lett.*, *19*, 1839–1842, 1992a.

Gaffen, D. J., A. Robock, and W. P. Elliott, Annual cycles of tropospheric water vapor, *J. Geophys. Res.*, *97*, 18,185–18,193, 1992b.

Gates, W. L., The Atmospheric Model Intercomparison Project, *Bull. Am. Meteorol. Soc.*, *73*, 1962–1970, 1992.

Gulev, S. K., I. I. Zveryayev, and I. I. Mokhov, Tropospheric lapse rate as a function of surface temperature conditions, *Izv. Acad. Sci. Russ., Atmos. Oceanic Phys.*, *27* (4), 287–294, 1991.

Hallberg, R., and A. K. Inamdar, Observations of seasonal variations in atmospheric greenhouse trapping and its enhancement at high sea surface temperature, *J. Clim.*, *6*, 920–930, 1993.

Hansen, J., A. Lacis, D. Rind, G. Russell, P. Stone, I. Fung, R. Ruedy, and J. Lerner, Climate sensitivity: Analysis of feedback mechanisms, in *Climate Process and Climate Sensitivity*, edited by J. E. Hansen and T. Takahashi, vol. 29 of *Geophys. Monogr. Ser.*, pp. 130–163, AGU, Washington, D. C., 1984.

Harrison, E. F., P. Minnis, B. R. Barkstrom, V. Ramanathan, R. D. Cess, and G. G. Gibson, Seasonal variations of cloud radiative forcing derived from the Earth's Radiation Budget Experiment., *J. Geophys. Res.*, *95*, 18,687–18,703, 1990.

Le Treut, H., and Z. X. Li, Sensitivity of an atmospheric general circulation model to prescribed SST changes: Feedback effects associated with the simulation of cloud optical properties., *Clim. Dyn.*, *5*, 175–187, 1991.

Liu, W. T., Statistical relation between monthly mean precipitable water and surface-level humidity over global oceans, *Mon. Weather Rev.*, *114*, 1591–1602, 1986.

Liu, W. T., W. Tang, and P. P. Niiler, Humidity profiles over the ocean, *J. Clim.*, *4*, 1023–1034, 1991.

Morcrette, J.-J., Impact of changes to the radiation transfer parameterizations plus cloud optical properties in the ECMWF model, *Mon. Weather Rev.*, *118*, 847–873, 1990.

Morcrette, J.-J., L. Smith, and Y. Fouquart, Pressure and temperature dependence of the absorption in longwave radiation parameterizations, *Beitr. Phys. Atmos.*, *59*, 455–469, 1986.

Prabhakara, C., G. Dalu, R. C. Lo, and N. R. Nath, Remote sensing of seasonal distribution of precipitable water over the oceans and the inference of boundary-layer structure, *Mon. Weather Rev.*, *107*, 1388–1401, 1979.

Raval, A., and V. Ramanathan, Observational determination of the greenhouse effect, *Nature*, *342*, 758–761, 1989.

Reynolds, R. W., A real-time global Sea Surface Temperature analysis, *J. Clim.*, *1*, 75–86, 1988.

Roberts, R. E., J. E. A. Selby, and L. M. Biberman, Infrared continuum absorption by atmospheric water vapour in the 8-12 micron window., *Appl. Opt.*, *15*, 2085–2090, 1976.

Rossow, W. B., and L. C. Garder, Validation of ISCCP cloud detections., *J. Clim.*, *6*, 2370–2393, 1993.

Rossow, W. B., and R. A. Schiffer, ISCCP cloud data products, *Bull. Am. Meteorol. Soc.*, *72*, 2–20, 1991.

Sadourny, R., and K. Laval, January and July performance of the LMD general circulation model, pp. 173–197, *New Perspectives in Climate Modelling*, edited by A. Berger and C. Nicolis, Elsevier, New-York, 1984.

Stephens, G. L., On the relationship between water vapor over the oceans and sea surface temperature, *J. Clim.*, *3*, 634–645, 1990.

Stephens, G. L., and T. J. Greenwald, Observations of the Earth's radiation budget in relation to atmospheric hydrology, 1, Clear-sky greenhouse effect and water vapor feedback, *J. Geophys. Res.*, *96*, 15,311–15,324, 1991.

Stone, P. H., and J. H. Carlson, Atmospheric lapse rate regimes and their parameterization, *J. Atmos. Sci.*, *36*, 415–423, 1979.

Sun, J., Effects of vertical distribution of water vapor and temperature on total column water vapor retrieval error, *J. Geophys. Res.*, *98*, 7069–7079, 1993.

Webb, M. J., A. Slingo, and G. L. Stephens, Seasonal variations of the clear-sky greenhouse effect: The role of changes in atmospheric temperatures and humidities, *Clim. Dyn.*, *9*, 117–129, 1993.

Wentz, F. J., A model function for ocean microwave brightness temperatures, *J. Geophys. Res.*, *88*, 1892–1908, 1983.

Wetherald, R. T., and S. Manabe, Cloud feedback processes in a general circulation model, *J. Atmos. Sci.*, *45* (8), 1397–1415, 1988.

Yang, S. K., and G. L. Smith, Further study on atmospheric lapse rate regimes, *J. Atmos. Sci.*, *42*, 961–965, 1985.

S. Bony, Laboratoire de Météorologie Dynamique du Centre National de la Recherche Scientifique, Ecole Normale Supérieure, 24 rue Lhomond, F-75231 Paris cedex 05, France (e-mail: bony@lmd.ens.fr).

J.-Ph. Duvel, Laboratoire de Météorologie Dynamique du Centre National de la Recherche Scientifique, Ecole Polytechnique, F-91128 Palaiseau cedex, France (e-mail: duvel@lmdx12.polytechnique.fr).

(Received July 6, 1993; revised January 11, 1994; accepted February 14, 1994.)